Nano Energy 33 (2017) 515–521

Contents lists available at ScienceDirect

Nano Energy

journal homepage: www.elsevier.com/locate/nanoen

Communication

Tandem triboelectric nanogenerators for optimally scavenging mechanical energy with broadband vibration frequencies

Divij Bhatia[a], Wook Kim[a], Sangmin Lee[b], Sang Woo Kim[c], Dukhyun Choi[a,*]

[a] Department of Mechanical Engineering, Kyung Hee University, Yongin 17104, South Korea
[b] Department of Mechanical Engineering, Chung-Ang University, Seoul 06974, South Korea
[c] School of Materials Science and Engineering, Sungkyunkwan University, Suwon 16419, South Korea

ARTICLE INFO

Keywords:
Triboelectric nanogenerator
Broadband vibration
Design protocol
Tandem system

ABSTRACT

Triboelectric nanogenerators (TENG) can effectively generate electrical energy from the otherwise wasted mechanical energy in our environment. However, since vibration energy scavengers are usually driven at their resonant frequency, vibrating TENGs (VTENG) can provide maximized output power only within a few Hz of input frequencies. Here, we report tandem TENGs which are able to optimally scavenge abundant vibration energy under a wide band of input frequencies (tens of Hz and beyond). We first investigate the dynamic response of a single VTENG by parametric analyses (external forces, mass, stiffness, and gap distance) according to input frequencies. Based on coupled behavior, we complete a design protocol for a single VTENG, providing optimal power generation at a given frequency. Finally, we demonstrate a tandem system of resonant VTENGs, where maximum output power can be produced over a broad range of input frequencies between 15 and 40 Hz. It is expected that our design protocol enables optimal energy conversion for an individual TENG and that tandem design will be practically useful for consistently scavenging a wide band of vibration energy from environmental sources such as vehicles, wind, and waves.

1. Introduction

Utilizing multiple forms of renewable energy becomes crucial as the world gradually moves away from relying on fossil fuels as a major energy resource. Water waves, blowing wind, human motion, and means of transportation are all examples of renewable vibration energy resources. Most of this vibration energy, however, is usually lost to heat and damping. We can recover this energy with devices that convert mechanical motion into electrical energy via piezoelectric [1–3], electrostatic [4,5], electrochemical [6], magnetostrictive [7], electromagnetic [8,9], and triboelectric [10–13] generator technologies, as well as via their hybrid combinations [14–16].

Vibration energy scavengers are usually designed as resonant systems; the oscillating frequency of a vibrating scavenger is tuned to match the vibration source frequency. This is because resonant systems can provide high speed and large amplitude motion, thus yielding the highest power output. However, since the working bandwidth of a resonant scavenger is normally narrow (a few Hz), any changes in input frequency conditions can easily cause frequency mismatch which leads to reduced performance. For this reason, a broadened output frequency response is sought by introducing nonlinearities in the system dynamics [3,9].

Recently, triboelectric nanogenerators (TENG), which rely on the coupling between triboelectrification and electrostatic induction for their operation [10], have been heavily researched due to their highly efficient mechanical to electrical energy conversion, and several innovative designs and potential applications, such as self-powered sensors have been proposed [17–21]. For harvesting ambient vibration energy, a variety of different TENG systems have been proposed [22–24] targeted for ocean wave motion [25,26], human motion [27,28], and acoustic energy [29,30] scavenging. Since the working mechanism of a vertical contact-mode TENG involves repeated contact and separation for energy production, the dynamics of a vibrating TENG (VTENG) are inherently non-linear, resulting in widened output frequency response [31–33]. Although some previous studies have shown resonant designs for VTENGs, their VTENGs were not specially designed for a predetermined frequency, and the dynamic coupling effects of internal and external variables (such as mass, gap distance, and force) were not considered. In order to ensure optimal operation of the VTENG, it is crucial to follow a resonant design protocol for a predetermined frequency after carefully studying the complex VTENG dynamics and parametric coupling effects. Furthermore, to effectively

* Corresponding author.
E-mail address: dchoi@khu.ac.kr (D. Choi).

http://dx.doi.org/10.1016/j.nanoen.2017.01.059
Received 30 November 2016; Received in revised form 29 January 2017; Accepted 31 January 2017
Available online 01 February 2017

harvest various wasted vibration energy from waves, wind, vehicles, and body movements with broadband input frequencies (over tens of Hz), a more strategic VTENG system design is necessary.

In this work, we introduce tandem TENG for harvesting vibration energy with a broadband frequency range (tens of Hz and beyond), through resonant system design of individual VTENGs at predetermined input frequencies. First, we show that our vibration model for a VTENG can yield a resonant system that generates highest output power in the range of a target frequency within a few Hz. Second, we demonstrate that tandem construction of VTENGs is critical to achieving optimal output energy in a broad input frequency range (working bandwidth of about 25 Hz). Because the control variables (external forces, gap distance, mass and stiffness) for the resonant design of a VTENG are coupled, parametric investigations are performed by simulating an impact vibration model that describes VTENG motion dynamics. Based on the simulation results and experimental verifications, we complete a systematic design protocol for the optimal resonant system of an individual VTENG. Finally, a tandem TENG is demonstrated to consistently provide maximum power at vibration frequencies of several tens of Hz.

2. Experimental methods

2.1. VTENG fabrication and operation

A schematic of the VTENG and operation flow is shown in Supplementary Fig. S1. The top and bottom substrates were 3D printed using Polylactic Acid (PLA). Commercial aluminum foil and polytetrafluoroethylene (PTFE), located at the positive and negative ends of the triboelectric series [34], respectively, were used as the tribologically-active (tribo-active) materials. PTFE film (80 μm thick) was glued to an aluminum foil electrode (16 μm thick). The tribo-active materials had a contact area of 3*3 cm^2. Four springs provided a natural separation between the PTFE and aluminum. The springs made no contact with the tribo-active and electrode materials. The top aluminum and bottom aluminum electrodes were fixed to the PLA substrates using commercial double-sided tape (polyethylene (PE) foam). The bottom substrate was fixed to the vibration input source; the top substrate was movable. The PTFE and aluminum were repeatedly placed in contact for several cycles in order to induce contact electrification and surface charge saturation. This ensured that the PTFE would now carry a constant negative surface charge. When the aluminum moved away from the PTFE, conventional current flowed between the aluminum electrodes due to electrostatic induction. Current flowed in the opposite direction when the aluminum moved towards the PTFE; thus, an alternating current flowed across the impedance, corresponding to the motion of the aluminum.

2.2. Vibration test measurements

The vibration test equipment setup and block diagram are shown in Supplementary Fig. S2. The VTENG bottom substrate was fixed atop a Labworks Inc. ET-126B electrodynamic shaker, which provided the input vibration. The amplitude of the input vibration was controlled with a preamplifier. Frequency sweep settings were controlled manually using a Tektronix AFG3021C function generator. The VTENG output voltage was measured using a Tektronix MDO3012 mixed domain oscilloscope with an input impedance of 10 MΩ. Current measurements were made using a Stanford Research Systems SR570 low-noise current preamplifier connected to the Tektronix MDO3012 mixed domain oscilloscope.

2.3. Simulation

VTENG natural vibration mode simulation was performed using ABAQUS/CAE finite element modeling software. The impact vibration model was simulated using MATLAB/Simulink software. The Simulink model is shown in Supplementary Fig. S3. Details of the model are provided as Supplementary information. Periodic sine wave frequency input was swept from 0 to 50 Hz using a "for" loop. Amplitude and velocity output values were collected in the MATLAB workspace. Here, the amplitude is defined as the maximum value of x(t) at each frequency, where x(t) is actual vibration oscillation motion, such as sinusoidal movement. Only the peak values from the output were identified and plotted versus the input frequency. The values used for ζ, ζ_1 and ω_1 were 0.003, 0.05, and 2π*100 rad/s, respectively (See Supplementary information for details on the impact vibration model).

3. Results and discussion

3.1. Design concept and strategy for tandem TENG

Our strategy for creating tandem TENG to harvest broadband vibration energy can be explained as follows. First, we examine the coupling effects of the control parameters by using a single VTENG; then the fundamental vibration theory is modified based on the coupling dynamics, resulting in a resonant design protocol for the VTENG at a predetermined input frequency. Finally, tandem VTENG structures are completed for optimized, high-output broadband vibration energy harvesting. This strategy is summarized in Supplementary Fig. S4. The tandem assembly configuration is flexible and scalable in three dimensions, thus, it can be either vertical, lateral or combination configuration as shown in Supplementary Fig. S5. Details are introduced below.

3.2. Importance of resonant design for VTENG

For the purpose of the resonance design of an individual VTENG, we consider the control parameters of a VTENG. Fig. 1a provides a detailed illustration of the VTENG structure and parameters. The VTENG bottom substrate is fixed to the vibration input source with input frequency, f_{in}. Let N springs with total stiffness Nk (here, N =4, and each spring has a stiffness of k) support the total movable mass, m, which consists of the mass of the top substrate m_{sub}, mass of the polyethylene (PE) foam layer, m_{poly}, and mass of the TENG positive material, m_{pos}, that also serves as the electrode, since it can normally be a conducting metal. The purpose of the foam layer is to provide improved contact interaction between the positive and negative materials (tribo-active materials). The thicknesses of the top foam layer and positive TENG material are t_{poly}, and t_{pos}, respectively. TENG negative material with thickness, t_{neg}, TENG bottom electrode with thickness, t_{elec}, and the bottom adjustable PE foam layer of thickness, t_{polyc}. are stacked on the bottom substrate. In this study, we used an aluminum foil as a positive and top electrode material and polytetrafluoroethylene (PTFE) as a negative material. By the material selection and treatment, the output performance can be changed and improved, but the resonant behavior should be same. The gap distance between the tribo-active materials is designed to be d_O after assembling. The original length of a single spring is L_O, while the spring length under the condition of system equilibrium after assembling changes to L due to the movable mass at the top. Based on these parametric definitions, the natural frequency of the VTENG, f_{sys}, can be given from,

$$2\pi f_{sys} = \sqrt{\frac{Nk}{m}}. \quad (1)$$

Fig. 1b describes the amplitude response characteristics of a VTENG. First, it shows that under the resonance condition (f_{in} = f_{sys}), the motion of total mass, m, is significantly greater than the out of resonance condition. Secondly, the behavior shows that if the amplitude is greater than d_O, an impact condition will result and the

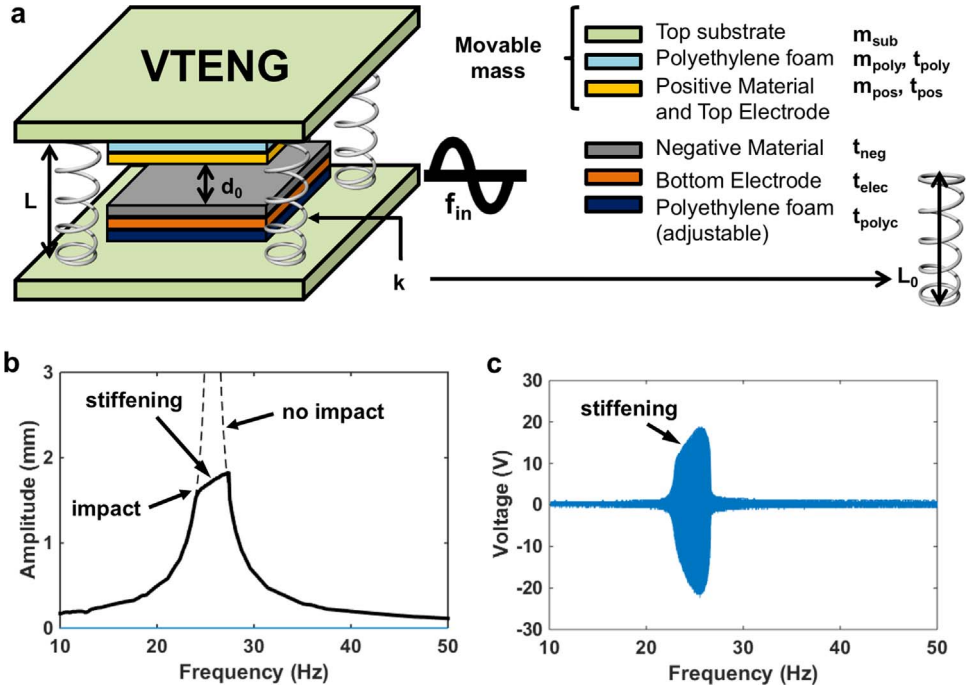

Fig. 1. Control parameters and resonant output behavior for VTENG. (a) Schematic of VTENG showing important design parameters. (b) Amplitude response simulation stiffening characteristic under impact condition. (c) Resonant output voltage response of VTENG with stiffening.

motion of mass, *m*, will be restricted by the gap distance, d_O. This flattening of the amplitude response is referred to as the stiffening [35] or hardening [36] characteristic. Stiffening is replicated in the experimental voltage response of the VTENG as shown in Fig. 1c. The upper part of the voltage response shows flattening due to the stiffening characteristic caused by the impact. Under non-resonance conditions, the voltage output of the VTENG is practically zero due to small amplitude oscillations; however, the voltage output is considerably higher at near resonance conditions due to large amplitude oscillations. The resonant behavior of current ouput from the VTENG is also the same. Thus the working bandwidth of a single VTENG is limited to a few Hz near its resonant frequency. This shows that resonance design approach to VTENGs is critical for obtaining optimal output power.

3.3. Theoretical understanding of coupled effects for VTENG

In order to clearly understand the coupling behaviors of the external and internal variables within a VTENG, we theoretically

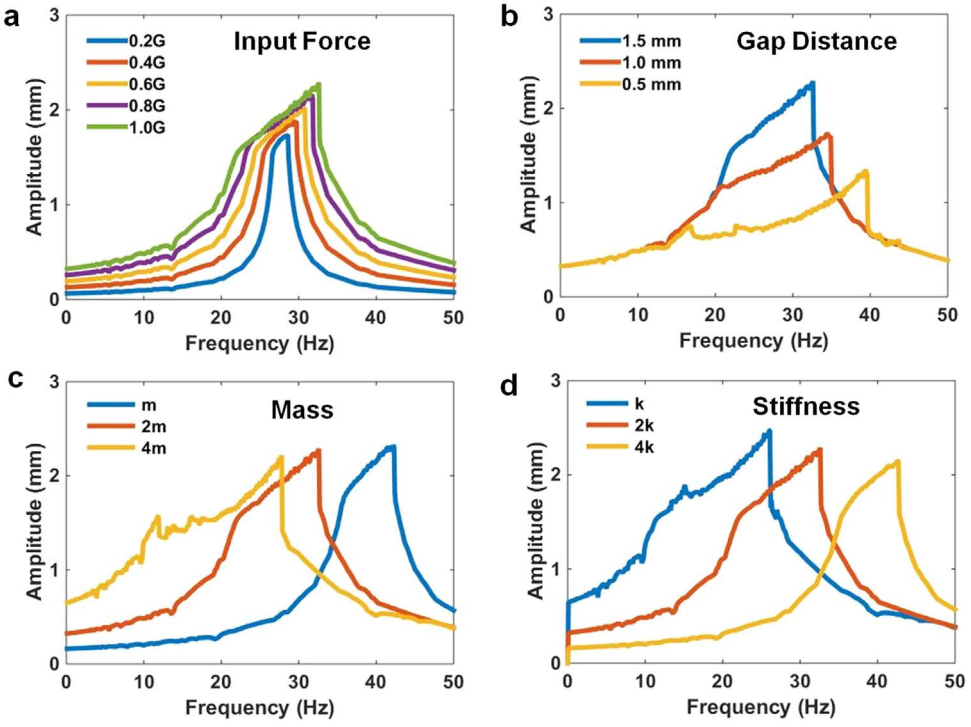

Fig. 2. Understanding of coupling effect for control parameters of VTENG via simulation. Amplitude response of VTENG when changing (a) input acceleration, (b) separation gap distance between the tribo-active materials, (c) moving mass, and (d) spring stiffness.

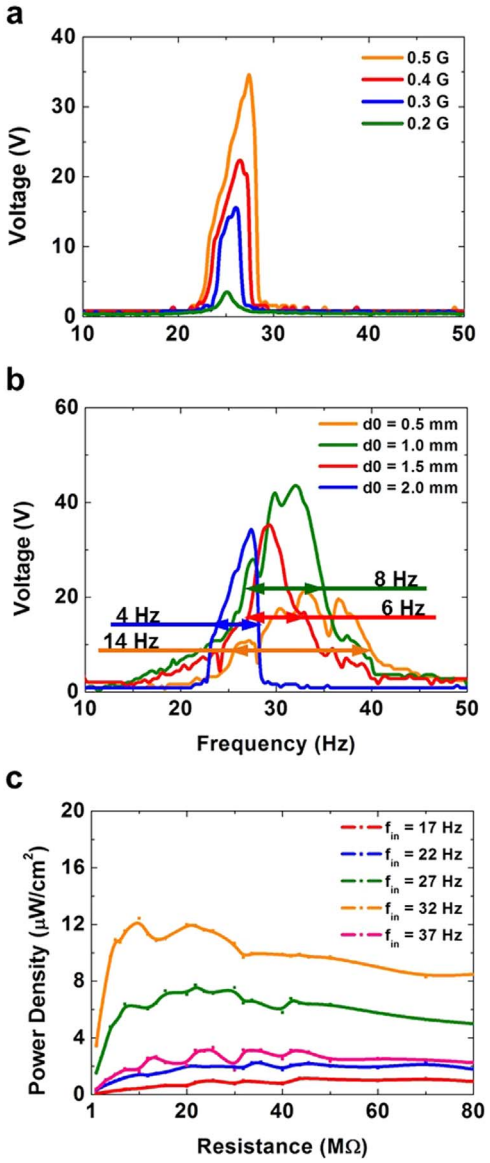

Fig. 3. Experimental investigations for critical control parameters of VTENG. Peak voltage response of VTENG when changing the (a) input acceleration and (b) separation gap distance (d_0) between the tribo-active materials. (c) Output power density curves at different input frequencies according to the load resistance, for d_0 =1 mm.

studied its nonlinear dynamics by utilizing an impact based vibration model [37]. The details of both the impact vibration model and the electrical model are described in the Supplementary information, in addition to a lumped model for the VTENG provided in Supplementary Fig. S6. The electrical model for the VTENG [38] shows that the open-circuit voltage depends on VTENG amplitude (see Equation (S6)), while the short-circuit current depends on VTENG amplitude and velocity (see Equation (S7)). Since the amplitude and velocity of the VTENG correlate directly with its output performance, we explore the amplitude and velocity response characteristics of the VTENG according to the control parameters of input force (F_{in}), gap distance (d_O), mass (m), and stiffness (k).

Fig. 2 shows the amplitude response simulation results, while the velocity response simulation results are provided in Supplementary Fig. S7 because the behaviors were almost similar. Fig. 2a demonstrates the effect of increasing the magnitude of the input force, F_O (acceleration, G) on the amplitude response. Higher peak amplitudes and increased working bandwidths were observed when the input acceleration was increased from 0.2 to 1 G. As an external variable, it is clear that higher input force increases the amplitude of the oscillating mass and correspondingly the amount of impact, thus providing greater output power and widening the VTENG operable frequency range.

Fig. 2b shows the effect of increasing the gap distance (d_O) from 0.5 to 1.5 mm. The amplitude at which the response begins to stiffen corresponds to the value of the gap distance, as expected. An increase in the working bandwidth was observed at lower values of d_O. This phenomenon can be explained by considering the various oscillation modes of the VTENG (see Supplementary Fig. S8 and supplementary Movie S1). Different VTENG oscillation modes occur at various input frequencies. At low values of d_O, even the small amplitude oscillation modes will cause an impact condition; thus if several oscillation modes lead to impact, the overall working bandwidth of the VTENG will increase at low d_O. However due to lower amplitude oscillation, the peak voltage output will decrease at low d_O. This trade-off for working bandwidth and voltage output, with respect to gap distance, is an important consideration in the optimal design of the VTENG. Thus, we expect that a tandem TENG will enable optimal broadband vibration energy harvesting if individual VTENGs are optimized to produce maximum output power at a predetermined but varied frequency ranges.

A simulation-based parametric study was performed for mass (m) and stiffness (k), as shown in Fig. 2c and d. From Eq. (1), we can conclude that increasing the mass decreases the VTENG system natural frequency (f_{sys}), while increasing the stiffness has the opposite effect. However, mass and stiffness also have an effect on the gap distance (d_O). If $\Delta L = L_0 - L$, considering the force balance for VTENG in a resting state yields,

$$mg = (Nk)\Delta L. \tag{2}$$

If all material thicknesses are grouped as: $t_m = t_{pos} + t_{poly} + t_{neg} + t_{elec} + t_{polyc}$, since $L = d_0 + t_m$, Eq. (2) can be modified to describe d_O in terms of m and k,

$$d_0 = L_0 - \frac{mg}{(Nk)} - t_m. \tag{3}$$

From Eq. (3) we can conclude that if the mass is increased, the gap distance will decrease, while increasing the stiffness will have the opposite effect. Thus the coupled effect of mass and stiffness on the VTENG natural frequency and gap distance are made clear from Eqs. (1) and (3). This coupled effect is illustrated in Supplementary Fig. S9.

Based on the above theory, we can explain the VTENG amplitude response simulation results for mass and stiffness changes as shown in Fig. 2c and d, respectively. Increasing the mass as m, $2\,m$, and $4\,m$ shifts the amplitude response curve leftward, since increasing the mass will reduce the VTENG natural frequency, while the working bandwidth increases in conjunction with increasing mass due to the reduced gap distance. Increasing the stiffness has the opposite coupling effect to the increasing mass, as explained above. In summary, the simulation results bring to light several control parameters which effect VTENG dynamics and have coupled effects. Increasing the input force increases the output as well as the working bandwidth, decreasing the gap distance can decrease the output but will increase working bandwidth, increasing the mass shifts the frequency of operation to a lower frequency while simultaneously increasing the working bandwidth, and increasing the spring stiffness shifts the frequency of operation to a higher frequency while simultaneously decreasing the working bandwidth of the VTENG.

3.4. Experimental verification of VTENG behaviors

To verify the simulation results, we experimentally investigated the coupling effects of the external (input force) and internal (gap distance) variables of a VTENG as shown in Fig. 3. Fig. 3a compares the output voltage results for changes in input acceleration at d_O =2.0 mm (note

that only the peak positive side outputs are shown for clarity, the actual alternating output data is provided as Supplementary Fig. S10). As the input acceleration was increased from 0.2 to 0.5 G in steps of 0.1 G, the peak voltage and working bandwidth increased throughout the frequency spectrum, as predicted by the simulation. Fig. 3b shows the peak output voltage results for changes in d_O at an input acceleration of 0.5 G (again, note that only the peak positive side outputs are shown for clarity, the actual alternating output data is provided as Supplementary Fig. S11). The full-width at half-maximum bandwidth at d_O =2.0 mm was 4 Hz, while the maximum output voltage was 34 V. At d_O =1.5 mm, the full-width at half-maximum bandwidth was 6 Hz, while the maximum output voltage was 35 V. At d_O =1.0 mm, the full-width at half-maximum bandwidth was 8 Hz, while the maximum output voltage was 44 V. Finally, at d_O =0.5 mm, the full-width at half-maximum bandwidth was 14 Hz, while the maximum output voltage was 22 V. As d_O was decreased, the frequency at which highest voltage was obtained shifted to the right, as predicted by the simulation results in Fig. 2b and Figure S7. Fig. 3c shows the power density results at different input frequencies for d_O =1.0 mm, with the VTENG resonant frequency (f_{sys}) being 27 Hz. Due to stiffening effects shown in Fig. 1, the highest power output was obtained at input frequency f_{in} =32 Hz. Thus, the results clearly show that the resonant conditions are important to provide the maximum output power. In agreement with the simulation results, our experimental results showed that small gap distances (d_O =0.5 mm) can widen the working frequency of VTENG but the peak output power decreases. By increasing the gap distance, we can increase the output power but it yields narrow bandwidth working frequency. Accordingly, we need a tandem TENG system to increase the working bandwidth while maintaining high power output by using resonant VTENGs at given working frequencies.

3.5. Design protocol for resonant VTENG

For optimal and strategic design of an individual VTENG, we utilized the resonance condition to estimate values of the design parameters. Since for resonance condition, $f_{sys} = f_{in}$, Eq. (1) can be modified to give spring stiffness as,

$$(Nk) = m*(2\pi f_{in})^2. \quad (4)$$

Furthermore, substituting Eq. (4) in Eq. (3) gives an estimate for the required length of a coil spring as,

$$L_0 = d_0 + \frac{g}{(2\pi f_{in})^2} + t_m. \quad (5)$$

Eq. (4) is graphically illustrated in Supplementary Fig. S12, which can be used as a design chart for determining the approximate values of mass or stiffness for a given input frequency. For a given input frequency, the required length of coil spring (L_O) can determined based on the gap distance (d_O) value. Once we know the required values for k and L_O from Eqs. (4) and (5), respectively, the final coil spring can be designed, which is critical to complete the resonance system of an individual VTENG.

By understanding the coupled behaviors of control parameters for an individual VTENG, we completed a design protocol illustrated in Fig. 4, for the resonant design of an individual VTENG. The protocol steps are described in figure-form by means of an example in Supplementary Fig. S13. Initially the target frequency for resonance design must be determined based on the vibration source input frequency (f_{in}). Then, the required spring stiffness (k) can be determined for a given mass (m) using Eq. (4). However, the required mass (m) can be determined if the spring stiffness (k) is fixed. Mass design is essentially a case of determining the volumetric dimensions of each layer that make up the total mass (m). Since $m = m_{sub}+m_{poly}+m_{pos}$, knowing the density ($\rho$) of the top substrate, polyethylene foam, and positive TENG material, the volume (V) of each layer may be determined via the formula, $V = m/\rho$. To design a coil spring with

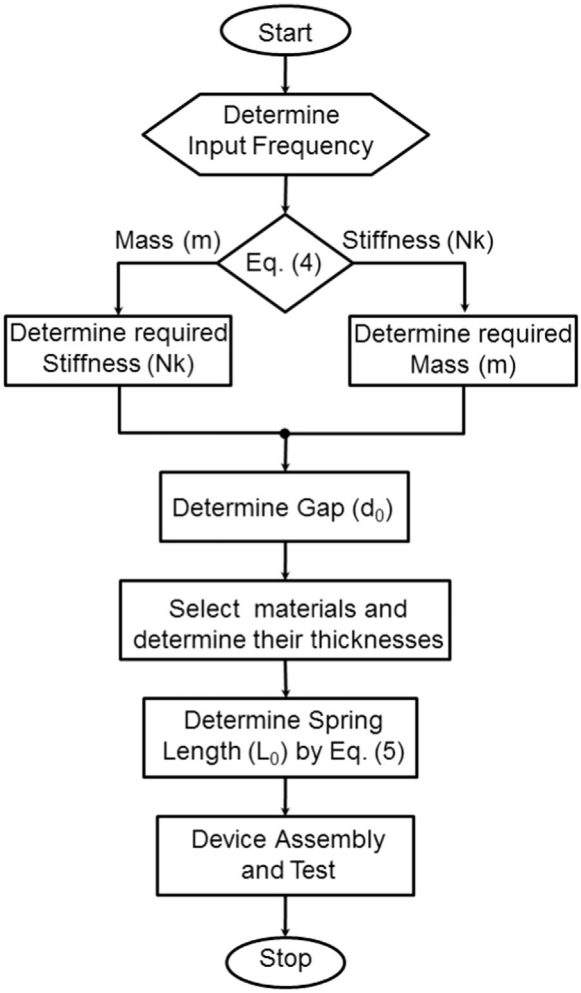

Fig. 4. Resonant design protocol for optimization of an individual VTENG. The design protocol is based on a modified vibration theory for maximizing the power output of the VTENG.

required stiffness, k, we can determine the required spring length from Eq. (5). However, the designer must first select the gap distance value (d_O). The impact vibration model simulation can only provide an estimate of the working bandwidth at a specific d_O. Since there is a trade-off in terms of d_O such that a lower d_O results in a lower peak voltage but a greater working bandwidth and vice-versa, therefore, the appropriate choice of d_O should be selected by the designer. Then the total material thickness, $t_m = t_{pos}+t_{poly}+t_{neg}+t_{elec}+t_{polyc}$, should be obtained and plugged into Eq. (5) to determine the required spring coil length (L_O). It must be stated that the values for material thickness and gap distance typically fall within a certain range, as given earlier. Furthermore, if there is a restriction in L_O, the thickness of the bottom polyethylene foam, t_{polyc}, may be suitably modulated as required. After completing the mass and spring design and selecting the materials, the VTENG can be assembled and tested. If further modification is required, the design protocol may be repeated from the necessary step onwards.

3.6. Design and fabrication of tandem TENG

We utilized the design protocol for creating a tandem system of individual resonant TENGs to harvest the broadband input vibration energy at high output power. Fig. 5a shows a vertical configuration tandem TENG consisting of four strategically designed VTENGs. Our goal was to cover the range of vibration input frequencies from 20 Hz to 40 Hz, with each VTENG providing maximum output power.

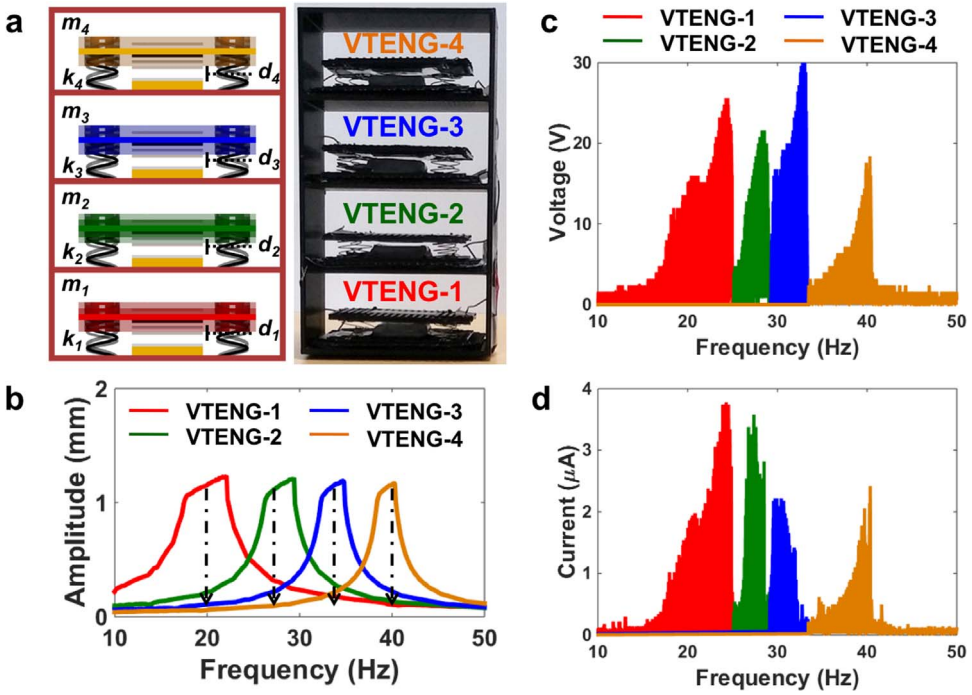

Fig. 5. Tandem TENG for scavenging vibration energy with broadband input frequencies. (a) Tandem TENG illustration of the assembled prototype. Four VTENGs are stacked in a vertical configuration to form tandem TENG. Each VTENG has specific mass, stiffness, and gap distance control parameters. (b) Amplitude response simulation for VTENGs based on an impact vibration model predicting wide-bandwidth output. (c) Voltage output response of tandem TENG. (d) Short-circuit current output response of tandem TENG.

Therefore, the input frequencies for the design protocol were selected as 20 Hz, 27 Hz, 34 Hz, and 40 Hz (a difference of approximately 7 Hz for every VTENG). Based on our resonant design protocol, we first determined movable mass (m) of 6.5g for each VTENG. Next, from Eq. (4), the required stiffness was determined to be approximately 100 N/m, 190 N/m, 295 N/m, and 410 N/m for k_1, k_2, k_3, and k_4, respectively, corresponding to VTENG-1, VTENG-2, VTENG-3, and VTENG-4. The impact vibration model simulation was performed at input acceleration of 0.2 G m/s^2 (lower than experimental conditions to accommodate for damping losses), and at fixed gap distance of 1 mm for all VTENGs. The amplitude response simulation of resonant VTENGs at each target frequency are shown in Fig. 5b and the velocity response simulation results are provided in Supplementary Fig. S14. The amplitude response simulation shows that our resonant TENGs can effectively scavenge vibration energy at the predetermined target frequencies with a total working bandwidth of upto 25 Hz (i.e. 15–40 Hz) due to impact stiffening characteristic of the VTENGs.

For VTENG fabrication, the top substrate was 3D printed using PLA material. We selected commercial aluminum foil as the bottom electrode and positive TENG material (t_{elec} = t_{pos} =16 μm), and PTFE film (t_{neg} =80 μm) as the negative TENG material. The top PE foam thickness was t_{poly} =2 mm, while the bottom PE foam thickness was modulated to obtain a fixed gap distance of d_0 =1 mm, since all of our coil spring lengths were restricted to 8 mm. Thus from Eq. (5), the bottom PE foam thickness was controlled at around t_{polyc} =4.5 mm for each resonant VTENG. Each VTENG was then assembled and individually tested. Finally, vertically-arranged tandem TENG was assembled and tested. The frequency sweep experiment was conducted at input acceleration of 0.5 G in order to clearly distinguish which VTENG was active (See Supplementary Fig. S15 and supplementary Movie S2). Fig. 5c shows the rectified voltage output results for tandem TENG, and Fig. 5d shows the rectified current output results. The output is color coded to represent VTENG-1, VTENG-2, VTENG-3, and VTENG-4 for ease of understanding. The peak output voltage ranges from 20 V to 30 V and the peak current ranges from 2 μA to 4 μA at input acceleration of 0.5 G. Normally the current and voltage output for VTENGs observed on an oscilloscope should follow similar trend. However, due to device-to-device variability, voltage output magnitude for VTENG-3 was higher than expected. Also, since our focus was primarily on the output bandwidth coverage we did not further investigate this minor anomaly. Thus, our fabricated and assembled tandem TENG covered the working bandwidth of 25 Hz (i.e. 15–40 Hz), as required. Thus, we confirmed that resonant VTENGs with optimal power could be successfully created by using our design protocol. Furthermore, it was demonstrated that tandem design of resonant VTENGs is critical for harvesting broadband vibration energies. Based on the target working bandwidth, we can freely change the number of required resonant VTENGs.

We further conducted an experiment at input acceleration of 1 G, as shown in Supplementary Fig. S16. The rectified peak output voltages observed in this case are beyond 100 V. An overlap in the working bandwidth was also observed, since the working bandwidth of each VTENG was increased due to high input force, as discussed earlier with the help of simulation and experimental based input force parametric analysis of a single VTENG. Additional improvements in tandem TENG output can be obtained by nanopatterning the tribo-active surfaces. The tandem TENG system can be arranged in a variety of configurations including vertical, lateral, and combination configurations, as shown in Supplementary Fig. S17. Thus, we demonstrated the viability of our method for optimal tandem TENG design, for harvesting wide-bandwidth vibration energy.

4. Conclusions

In summary, we introduced tandem TENG for scavenging environmental mechanical vibration energy with broadband input frequencies. For the purpose of optimal tandem TENG design, each VTENG was strategically designed by following a resonance design protocol. First, the vibration theory was modified for VTENG design based on resonance. Then the resonance design protocol was completed after systematically studying the parametric coupling effects via impact vibration model simulation and experimental verification. Each individual resonant VTENG constructed following the design protocol provides maximum power, but only within a few Hz of the predeter-

mined input frequency. Multiple resonant VTENGs were therefore designed to work collectively in tandem to scavenge wide-band input frequencies (tens of Hz) at maximum power. Since tandem TENG can be arranged in a variety of configurations, their design is flexible and scalable in three dimensions and they can be easily molded to suit any vibration energy harvesting application including wind, waves, and transportation.

Acknowledgements

This research was financially supported by the Fundamental Technology Research Program (2014M3A7B4052202), the Basic Research Laboratory Program (2016R1A4A1012950) and by the International Cooperation Program (2015K2A2A7056357) through the National Research Foundation of Korea (NRF) grant funded by the Ministry of Science, ICT and Future Planning (MSIP).

Appendix A. Supporting information

Supplementary data associated with this article can be found in the online version at doi:10.1016/j.nanoen.2017.01.059.

References

[1] L. Lin, Q. Jing, Y. Zhang, Y. Hu, S. Wang, Y. Bando, R.P.S. Han, Z.L. Wang, Energy Environ. Sci. 6 (2013) 1164–1169.
[2] K.B. Singh, V. Bedekar, S. Taheri, S. Priya, Mechatronics 22 (2012) 970–988.
[3] G. Sebald, H. Kuwano, D. Guyomar, B. Ducharne, Smart Mater. Struct. 20 (2011) 102001.
[4] S. Roundy, P.K. Wright, J. Rabaey, Comput. Commun. 26 (2003) 1131.
[5] P.D. Mitcheson, E.M. Yeatman, G.K. Rao, A.S. Holmes, T.C. Green, Proceedings IEEE, 96 (2008) 1457–1486.
[6] S. Kim, S.J. Choi, K. Zhao, H. Yang, G. Gobbi, S. Zhang, J. Li, Nat. Commun. 7 (2016) 10146.
[7] L. Wang, F.G. Yuan, Smart Mater. Struct. 17 (2008) 045009.
[8] K. Ashraf, M.M. Khir, J.O. Dennis, Z. Baharudin, Sens. Actuators A Phys. 195 (2013) 123–132.
[9] R.L. Harne, K.W. Wang, Smart Mater. Struct. 22 (2013) 023001.
[10] G. Zhu, B. Peng, J. Chen, Q. Jing, Z.L. Wang, Nano Energy 14 (2015) 126–138.
[11] S. Niu, X. Wang, F. Yi, Y.S. Zhou, Z.L. Wang, Nat. Commun. 6 (2015) 8975.
[12] S.B. Jeon, D. Kim, M.L. Seol, S.J. Park, Y.K. Choi, Nano Energy 17 (2015) 82–90.
[13] N. Cui, L. Gu, J. Liu, S. Bai, J. Qiu, J. Fu, X. Kou, H. Liu, Y. Qin, Z.L. Wang, Nano Energy 15 (2015) 321–328.
[14] H. Kim, S.M. Kim, H. Son, H. Kim, B. Park, J. Ku, J.I. Sohn, K. Im, J.E. Jang, J.J. Park, O. Kim, S.N. Cha, Y.J. Park, Energy Environ. Sci. 5 (2012) 8932–8936.
[15] J. Chen, Y. Huang, N. Zhang, H. Zou, R. Liu, C. Tao, X. Fan, Z.L. Wang, Nat. Energy 1 (2016) 16138.
[16] B. Zhang, J. Chen, L. Jin, W. Deng, L. Zhang, H. Zhang, M. Zhu, W. Yang, Z.L. Wang, ACS Nano 10 (2016) 6241–6247.
[17] H. Yong, J. Chung, D. Choi, D. Jung, M. Cho, S. Lee, Sci. Rep. 6 (2016) 33977.
[18] S. Lee, J. Chung, D.Y. Kim, J.Y. Jung, S.H. Lee, S. Lee, A.C.S. Appl, Mater. Interfaces 8 (2016) 25014–25018.
[19] S. Wang, L. Lin, Z.L. Wang, Nano Energy 11 (2015) 436–462.
[20] P. Bai, G. Zhu, Q. Jing, J. Yang, J. Chen, Y. Su, J. Ma, G. Zhang, Z.L. Wang, Adv. Funct. Mater. 24 (2014) 5807–5813.
[21] J. Yang, J. Chen, Y. Su, Q. Jing, Z. Li, F. Yi, X. Wen, Z. Wang, Z.L. Wang, Adv. Mater. 27 (2015) 1316–1326.
[22] H. Zhang, Y. Yang, Y. Su, J. Chen, K. Adams, S. Lee, C. Hu, Z.L. Wang, Adv. Funct. Mater. 24 (2014) 1401–1407.
[23] W. Yang, J. Chen, G. Zhu, X. Wen, P. Bai, Y. Su, Y. Lin, Z.L. Wang, Nano Res. 6 (2013) 880–886.
[24] Y. Hu, J. Yang, S. Niu, W. Wu, Z.L. Wang, ACS Nano 8 (2014) 7442–7450.
[25] Y. Hu, J. Yang, Q. Jing, S. Niu, W. Wu, Z.L. Wang, ACS Nano 7 (2013) 10424–10432.
[26] J. Chen, J. Yang, Z. Li, X. Fan, Y. Zi, Q. Jing, H. Guo, Z. Wen, K.C. Pradel, S. Niu, Z.L. Wang, ACS Nano 9 (2015) 3324–3331.
[27] W. Yang, J. Chen, G. Zhu, J. Yang, P. Bai, Y. Su, Q. Jing, X. Cao, Z.L. Wang, ACS Nano 7 (2013) 11317–11324.
[28] L. Jin, J. Chen, B. Zhang, W. Deng, L. Zhang, H. Zhang, X. Huang, M. Zhu, W. Yang, Z.L. Wang, ACS Nano 10 (2016) 7874–7881.
[29] X. Fan, J. Chen, J. Yang, P. Bai, Z. Li, Z.L. Wang, ACS Nano 9 (2015) 4236–4243.
[30] J. Yang, J. Chen, Y. Liu, W. Yang, Y. Su, Z.L. Wang, ACS Nano 8 (2014) 2649–2657.
[31] J. Chen, G. Zhu, W. Yang, Q. Jing, P. Bai, Y. Yang, T.C. Hou, Z.L. Wang, Adv. Mater. 25 (2013) 6094–6099.
[32] W. Yang, J. Chen, Q. Jing, J. Yang, X. Wen, Y. Su, G. Zhu, P. Bai, Z.L. Wang, Adv. Funct. Mater. 24 (2014) 4090–4096.
[33] J. Yang, J. Chen, Y. Yang, H. Zhang, W. Yang, P. Bai, Y. Su, Z.L. Wang, Adv. Energy Mater. 4 (2014) 1301322.
[34] A.F. Diaz, R.M. Felix-Navarro, J. Electrostat 62 (2004) 277–290.
[35] L. Dhakar, F.E.H. Tay, C. Lee, J. Micromech. Microeng. 24 (2014) 104002.
[36] K. Suhaimi, R. Ramlan, A. Putra, Adv. Acoust. Vib. 2014 (2014) 217032.
[37] H. Liu, C. Lee, T. Kobayashi, C.J. Tay, C. Quan, Smart Mater. Struct. 21 (2012) 035005.
[38] S. Niu, S. Wang, L. Lin, Y. Liu, Y.S. Zhou, Y. Hu, Z.L. Wang, Energy Environ. Sci. 6 (2013) 3576–3583.

Divij Bhatia is currently pursuing his Ph.D. at the Department of Mechanical Engineering in Kyung Hee University, Yongin, South Korea where he is a scholarship recipient from the Korean Government Scholarship Program. He has a Master of Science degree in Electrical Engineering from the Pennsylvania State University, USA and Bachelor of Engineering degree in Electronics and Telecommunications from the University of Mumbai, India. He is interested in renewable energy system design, optimization and implementation.

Wook Kim has a Master of Science degree in Mechanical Engineering from Kyung Hee University, Yongin, South Korea and is currently pursuing a Ph.D. under the supervision of Dr. Dukhyun Choi, Kyung Hee University. His research focuses on triboelectric nanogenerator fabrication and system design for efficient energy harvesting and self-powered systems.

Sangmin Lee received his Ph.D. in Mechanical Engineering from Pohang University of Science and Technology (POSTECH) in 2011. Now he is an assistant professor in the School of Mechanical Engineering at Chung-Ang University. His main research interests focus on the fields of piezoelectric and triboelectric nanogenerator for energy harvesting device and self-powered active sensor, super-flexible piezoelectric nanogenerator for self-powered/active sensor, surface wetting control including superhydrophobicity/superhydrophilicity based on micro/nanofabrications and their applications, mechanical characterization of micro/nanostructured surface.

Prof. Sang-Woo Kim is an Associate Professor in School of Advanced Materials Science and Engineering at Sungkyunkwan University (SKKU). He received his Ph.D. from Kyoto University, Department of Electronic Science and Engineering in 2004. After working as postdoctoral researcher at Kyoto University and University of Cambridge, he spent 4 years as assistant professor at Kumoh National Institute of Technology. He joined the SKKU Advanced Institute of Nanotechnology (SAINT) in 2009. His research is focused on piezoelectric/triboelectric nanogenerators, photovoltaics, and 2D nanomaterials. He is the Associate Editor of Nano Energy and an Executive Board Member of Advanced Electronic Materials.

Dukhyun Choi received his Ph.D. in Mechanical Engineering from Pohang University of Science and Technology (Postech) in 2006. From 2006–2008, he was a postdoctoral fellow with Dr. Luke P. Lee at UC Berkeley. Dr. Choi moved to Samsung Advanced Institute of Technology (SAIT) as a research staff. Since 2010, he is a Professor in Department of Mechanical Engineering at Kyung Hee University. His research interests include Energy Harvester, Plasmonics, Hybrid Photovoltaics, Flexible Electronics, and Water Splitting. Details can be found at: http://dchoi.khu.ac.kr.